Available online at www.sciencedirect.com
ScienceDirect
International Journal of Thermal Sciences 47 (2008) 1464–1472
International Journal of Thermal Sciences
www.elsevier.com/locate/ijts

Optimization of a staggered dimpled surface in a cooling channel using Kriging model

Kwang-Yong Kim *, Dong-Yoon Shin

Department of Mechanical Engineering, Inha University, Incheon 402-751, Republic of Korea

Received 2 February 2007; received in revised form 12 November 2007; accepted 19 December 2007

Available online 28 January 2008

Abstract

This study presents a numerical procedure to optimize the shape of staggered dimpled surface to enhance turbulent heat transfer in a rectangular channel. Kriging model based optimization technique is used with Reynolds-averaged Navier–Stokes analysis of fluid flow and heat transfer with shear stress transport turbulence model. The dimple depth-to-dimple print diameter ratio, channel height-to-dimple print diameter ratio, and dimple print diameter-to-pitch ratio are chosen as design variables. The objective function is defined as a linear combination of heat transfer and friction loss related terms with a weighting factor. Latin Hypercube Sampling is used to determine the training points as a mean of design of experiment. In the sensitivity analysis, it is found that the objective function is most sensitive to the ratio of dimple depth to dimple print diameter. Optimal values of the design variables have been obtained in a range of the weighting factor.

Keywords: Optimization; Dimple; Heat transfer; Kriging model; RANS analysis; Latin Hypercube Sampling; Objective function

1. Introduction

Among the heat transfer augmentation devices in internal cooling passages of turbine blades, such as ribs, dimples, pin-fins, etc., dimples have a characteristic of low-pressure drop penalty since there is no protrusion into the flow to produce significant pressure drag. The physical mechanism for the heat transfer augmentation with an array of dimples are the reattachment of the shear layer, the vortex structures and vertical fluid shedding from each individual dimple indentation, and the periodic unsteadiness which is produced as flow is ejected and then inrushes to each dimple.

Several papers were contributed on turbine cooling passage heat transfer enhancement problem in recent years. Ligrani et al. [1] reviewed the turbulent heat transfer enhancement techniques, such as ribs, pin-fins, dimples, etc. in internal flow passages like turbine blades. Mahmood and Ligrani [2] reported that the heat transfer is augmented as the ratio of channel height to dimple print diameter decreases. On the other hand, it was found in the experiments of Burgess and Ligrani [3] that the heat transfer rate also increases as the ratio of dimple depth to dimple print diameter increases. Park et al. [4] predicted turbulent flows in a channel with dimples. Their steady-state results show centrally located vortex pairs and vortex pairs located near the spanwise edges of individual dimples. Heat transfer and fluid flow characteristics for seven different dimpled surfaces on one surface of a channel are predicted numerically by Park and Ligrani [5], and they showed that the most significant local and overall heat transfer increases for spherical and tilted cylinder dimples.

These studies, however, does not report on the effect of the geometric parameters on thermal performance of dimpled channel in a systematic way, but only found the optimal case for better thermal performance among only a few tested cases. However, Kim and Choi [6] performed shape optimization of an in-line dimpled channel to enhance turbulent heat transfer using response surface method, and they showed the sensitivities of objective functions to design variables. Rib-roughened channel heat transfer optimizations using response surface approximation were performed by Kim and Kim [7] and Kim and Lee [8].

* Corresponding author. Tel.: +82 32 872 3096; fax: +82 32 868 1716.
E-mail address: kykim@inha.ac.kr (K.-Y. Kim).

1290-0729/$ – see front matter
doi:10.1016/j.ijthermalsci.2007.12.011

Nomenclature

A_d, A_{in}	areas of heat transfer surface and inlet plane, respectively
D	dimple diameter
D_h	channel hydraulic diameter
F	objective function
f	friction factor
H	channel height
Nu	local Nusselt number
Nu_a	average Nusselt number
Pi	dimple pitch
p, Δp	pressure and pressure drop in a channel, respectively
$\hat{p}$	periodic component of pressure
q_0	wall heat flux
Re	Reynolds number ($= U_b D_h/\nu$)
S	distance between dimples
T	local mean temperature
$\hat{T}$	periodic component of temperature
U_i	mean velocity components ($i = 1, 2, 3$)
U_b	averaged axial velocity at inlet
x, y, z	streamwise, spanwise, and cross-streamwise coordinates, respectively
x_i	coordinates ($i = 1, 2, 3$)

Greek symbols

β	weighting factor in objective function
γ	pressure gradient in streamwise direction
ν	kinematic viscosity
ρ	fluid density
σ	increasing rate of bulk temperature in axial direction
δ_{ij}	Kronecker delta ($i, j = 1, 2, 3$)

With the aid of high performance computers, numerical optimization techniques based on Reynolds-averaged Navier–Stokes analysis have been developed rapidly in the last decades. Among the methods of numerical optimization, such as response surface approximation, radial basis neural network, and Kriging models developed thus far, the Kriging model [9] is becoming popular for approximating deterministic computer models as it provides the best linear unbiased predictor. Kriging methods have been widely used to approximate the response of many deterministic computer models. Kriging model was applied to the design and analysis of computer experiments (DACE) by Sacks et al. [9]. Booker [10] used the Kriging model to study the aero-elastic and dynamic response of a helicopter rotor. Guinta [11] performed a preliminary investigation into the use of Kriging for the multidisciplinary design optimization of a high speed civil aircraft. Recently, Park et al. [12] used the Kriging for the optimization of a heat sink.

In this work, a shape optimization of a channel with single surface roughened by staggered dimples has been performed to maximize the performance of dimpled channel by compromising between heat transfer enhancement and reduction of friction loss. Kriging model is employed as an optimization technique to maximize thermal performance of the surface with three geometric design variables. Reynolds-averaged Navier–Stokes (RANS) analysis is used to evaluate the objective function by calculating turbulent convective heat transfer.

2. Numerical analysis

For steady three-dimensional RANS analysis of fluid flow and convective heat transfer in a dimpled channel, CFX-11.0 [13] which employs unstructured grids, is used in this work.

To adopt periodic boundary conditions, modifications of source terms in streamwise momentum and energy equations have been made to calibrate the gradual decrease and increase of pressure and temperature, respectively. Finally, for three-dimensional steady incompressible flows, mass, momentum, and energy conservation equations in tensor form can be written as follows;

$$\frac{\partial U_i}{\partial x_i} = 0 \tag{1}$$

$$U_j \frac{\partial U_i}{\partial x_j} = \frac{\partial}{\partial x_j}\left[\nu \frac{\partial U_i}{\partial x_j}\right] - \frac{1}{\rho}\frac{\partial \hat{p}}{\partial x_i} + \gamma \delta_{1i} \tag{2}$$

$$\frac{\partial}{\partial x_j}(\rho c_p U_j \hat{T}) = \frac{\partial}{\partial x_j}\left[k \frac{\partial \hat{T}}{\partial x_j}\right] - \sigma U_j \delta_{1j} \tag{3}$$

where $\hat{p}(x, y, z)$ and $\hat{T}(x, y, z)$ are the pressure and temperature transformed as follows in order to use the periodic boundary conditions [14] in streamwise direction, x.

$$\hat{p}(x, y, z) = p(x, y, z) + \gamma x \tag{4}$$

$$\hat{T}(x, y, z) = T(x, y, z) - \sigma x \tag{5}$$

Here, γ is the pressure gradient along the streamwise direction, and σ is the rate of bulk temperature increase due to wall heat flux, q_0.

$$\sigma = \frac{q_0 A_d}{\rho c_p Pi U_b A_{\text{in}}} \tag{6}$$

As a turbulence closure, Shear Stress Transport (SST) turbulence model reported by Menter [15] is employed with automatic wall treatment. SST model combines the advantages of the k-ε and k-ω models with a blending function. The k-ω model is activated in the near-wall region, and the k-ε model is used in the rest region. Bardina et al. [16] showed that the SST model captures separation under adverse pressure gradient well compared to other eddy viscosity models, and, thus, predicts well the near-wall turbulence that plays a vital role in the accurate prediction of turbulent heat transfer. Numerical model of Lai et al. [17] is adopted for modeling of turbulent heat flux.

High resolution schemes are used in discretization of the equations, and SIMPLE algorithm is employed in solution procedure. Relaxation factors are not introduced in iteration proce-

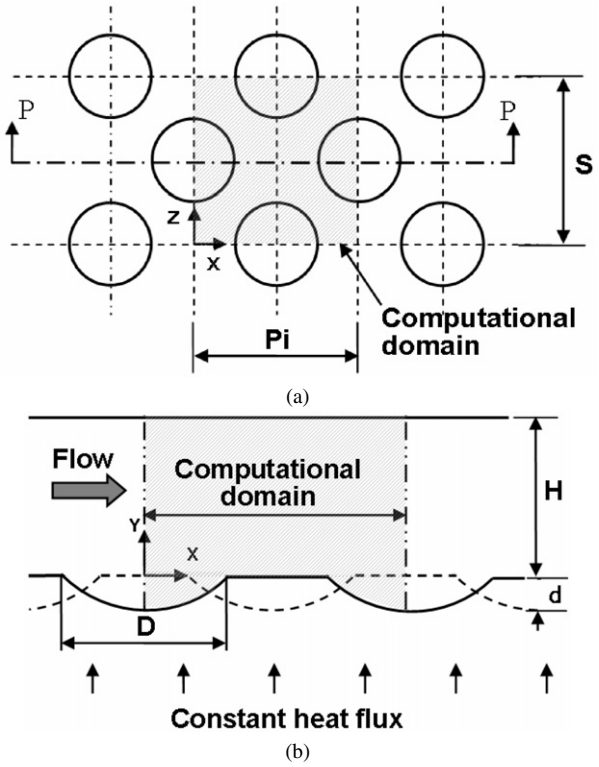

Fig. 1. Geometry and design variables.

dure. As convergence criteria for momentum and energy equations, the relative residuals are set to be less than 10^{-6}.

The computational domain contains four-half dimples as shown in Fig. 1. Periodic boundary conditions are used at all of the boundaries except the wall boundaries. Thus, the analyses are able to capture the asymmetric structure of the flow in dimple. An example of the grid system is shown in Fig. 2 for the whole computational domain and also, near the dimple wall. Unstructured tetrahedral grid system is used with the hexahedral at the wall region to resolve high velocity gradient. First grid points adjacent to walls are placed at $0.0002H$ from the walls to satisfy $y+$ less than 1.0, which is required to implement low-Reynolds number version of SST model. The number of grids node changes with the shape of dimples from 210 to 330 thousands.

In the present calculation, uniform heat flux is specified on the dimpled surface and the other flat walls are assumed to be adiabatic. Bulk velocity and constant temperature are set at all computational nodes as initial values to help the faster convergence of the iterative calculation.

The computations were carried out using personal computer, Intel Pentium IV CPU 3.0 GHz. The computational time for a single flow analysis is in the range of 18–24 hours depending upon the geometry considered and the convergence rate.

3. Optimization techniques

The optimization procedure is presented as a flow chart in Fig. 3. First, the objective function and design variables are selected. The design space is then decided for improved system performance. Using a suitable sampling scheme as the mean of

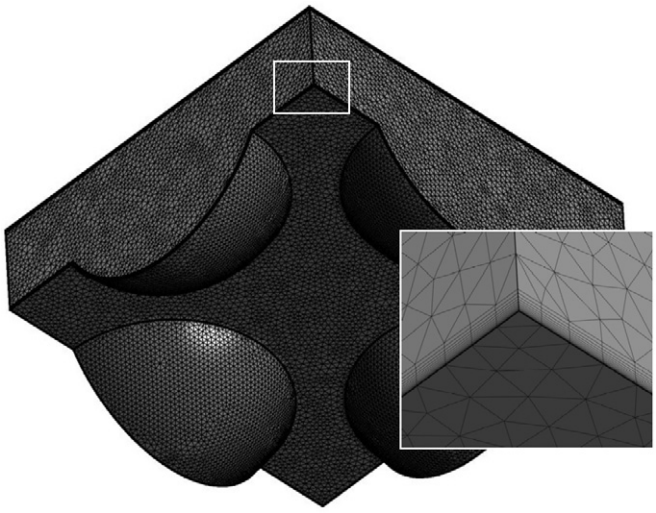

Fig. 2. Example of the grid system.

Design of Experiment, the design points are then obtained. At these design points, the objective function is calculated using a flow solver. Finally, the surrogate, i.e. the Kriging model, is constructed, and then optimal points are searched by the optimal point search algorithm. Each step is explained in detail in the following subsections.

3.1. Objective function and design variables

The optimization problem is defined as minimization of an objective function, $F(\boldsymbol{x})$ with $x_i^l \leqslant x_i \leqslant x_i^u$, where $\boldsymbol{x}$ is a vector of design variables, and x_i^l and x_i^u are lower and upper bounds of each design variable, respectively.

To maximize the performance of dimples, the optimal shape should be determined by a compromise between the enhancement of heat transfer and reduction in the friction loss. Therefore, the following definition of objective function used in the previous works [6–8,18,19] is employed in this work.

$$F = F_{Nu} + \beta F_f \tag{7}$$

where, β is the weighting factor. This factor should be determined by the designer considering the overall energy economy of the system. The first term on the right-hand side is defined as inverse of the average Nusselt number.

$$F_{Nu} = \frac{1}{Nu_a} \tag{8}$$

where,

$$Nu_a = \frac{\int_A \frac{Nu}{Nu_s}\,\mathrm{d}A}{A}$$

$$Nu_s = 0.023 Re^{0.8} Pr^{0.4}$$

Nu_s is the Nusselt number obtained from the Dittus–Boelter correlation, which is for the fully developed turbulent flows in a smooth pipe, and the integration is performed over the heated surface, A.

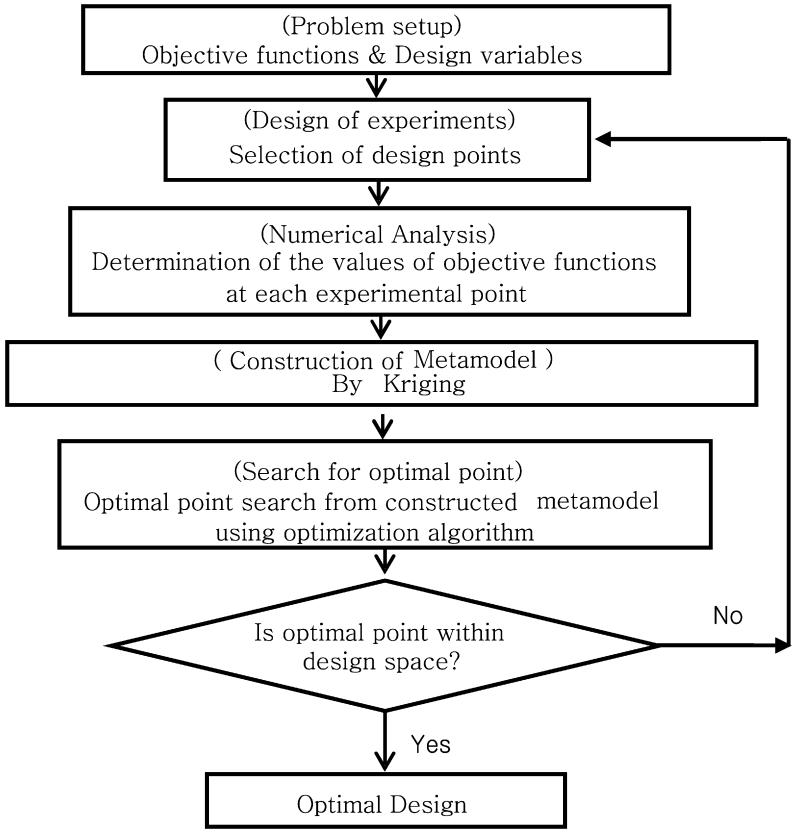

Fig. 3. Flow chart showing optimization procedure.

The second term which is related to friction loss is defined as follows;

$$F_f = \left(\frac{f}{f_0}\right)^{1/3} \tag{9}$$

where,

$$f = \frac{\Delta p D_h}{2\rho U_b^2 Pi}$$

$$f_0 = 2(2.236 \ln Re - 4.639)^{-2}$$

f_0 is a friction factor for fully developed flow in a smooth pipe, and is obtained from Petukhov empirical correlation [20] which is modified from the Karman–Nikuradse correlation for the best fit in the range, $10^4 < Re < 10^6$.

The channel with single surface roughened by staggered dimples is shown in Fig. 1. With five geometric parameters, i.e., channel height (H), dimple print diameter (D), dimple depth (d), distance between dimples (S), and dimple pitch (Pi), four dimensionless variables are found; H/D, d/D, D/S, and S/Pi. In the present optimization, S/Pi is set to be 1.0 to reduce the number of design variables. Therefore, three design variables such as H/D, d/D, and D/S are selected as design variables in the optimization.

3.2. Latin Hypercube Sampling (LHS)

In order to build the surrogate model, some experimental points are required for space filling of the design space. These can be established through the experiment design. Latin Hypercube Sampling (LHS) [21], an effective sampling method in DACE, is a matrix of $m \times n$ order, where m is the number of levels (sampling points) to be examined and n is the number of design variables. Each of the n columns of the matrix containing the levels $1, 2, \ldots, m$ is randomly paired to form a Latin hypercube. It generates random sample points, ensuring that all portions of the design space are represented.

3.3. Kriging method

The Kriging method [9] in its basic formulation estimates the value of a function (response) at some unsampled location as a combination of two components, the global model and a systematic departure. Mathematically,

$$y(x) = f(x) + Z(x) \tag{10}$$

where $y(x)$ is the unknown function to be estimated and $f(x)$ is a known function (usually polynomial) representing the trend over the design space, also referred to as the 'global' model. The second part, $Z(x)$, creates a localized deviation to interpolate the sampled data points by quantifying the correlation of points with a Gaussian correlation having zero mean and nonzero covariance. The covariance matrix of $Z(x)$ is given by

$$\operatorname{cov}\left[Z(x^i), Z(x^j)\right] = \sigma^2 \boldsymbol{R}\left[R(x^i, x^j)\right], \quad i, j = 1, 2, \ldots, n_s \tag{11}$$

where $\boldsymbol{R}$ is a correlation matrix consisting of a spatial correlation function (SCF), $R(x^i, x^j)$ as its elements. σ^2 is the process

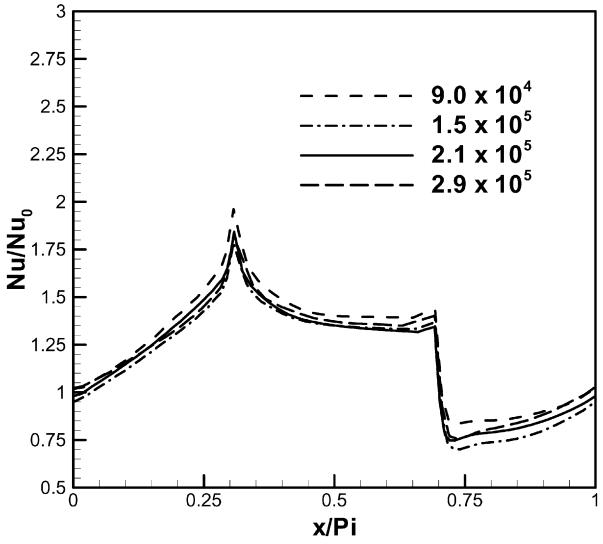

Fig. 4. Grid dependency test.

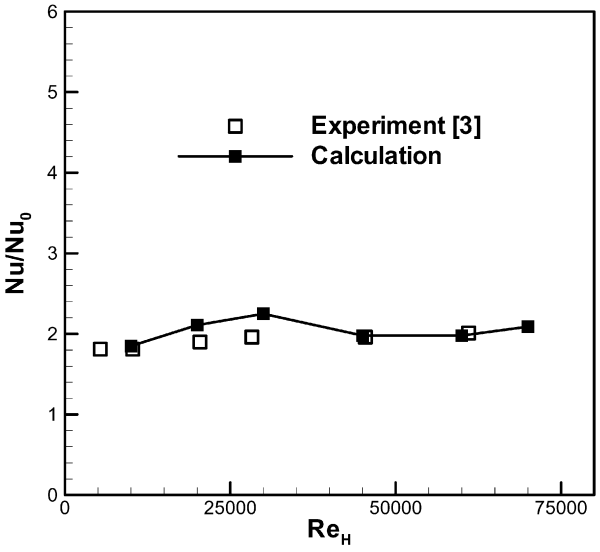

Fig. 5. Comparison between predicted and measured average Nusselt numbers.

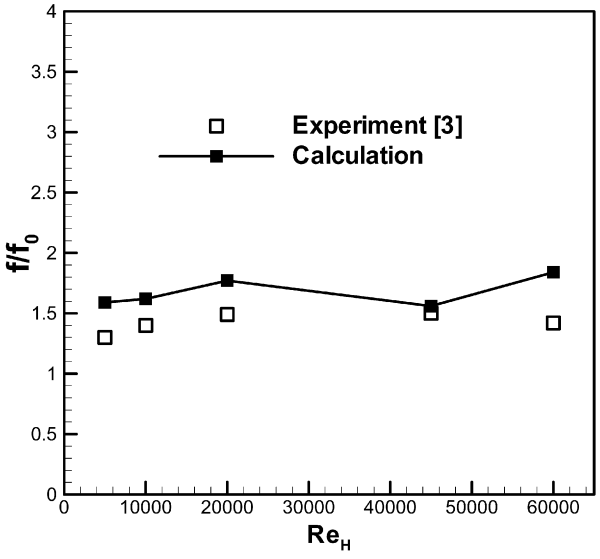

Fig. 6. Comparison between predicted and measured average friction factors.

variance representing the scalar of the spatial correlation function quantifying the correlation between any two n_s sampled data points x^i and x^j, and thereby controls the smoothness of the Kriging model, the effect of nearby points, and differentiability of the surface. The Gaussian function used in this work is the most preferable SCF when used with a gradient based optimization algorithm as it provides a relatively smooth and infinitely differentiable surface.

3.4. Optimization algorithm

Sequential quadratic programming (SQP) (function *fmincon* in MATLAB [22]) has been used as an optimization algorithm that follows Newton's method for constrained optimization in the manner of an unconstrained optimization problem. In its basic form it replaces the objective function with a quadratic approximation and replaces the constraint function by linear approximation. Its implementation consists of three steps, i.e., updating the Hessian matrix of the Lagrangian function using a quasi-Newton updating method, solution of the quadratic programming subproblem, and the formation of a search direction for a line search procedure using a line search and merit function calculation.

4. Results and discussion

Grid-dependency test has been performed for the staggered dimpled channel tested by Burgess and Ligrani [3] to determine the optimum grids as in Fig. 4 for streamwise Nusselt number distributions. The optimum number of grids has been selected as 210,000 from these results in this case. To validate the numerical solutions, calculated average Nusselt numbers on dimpled surface are compared with the experimental data of Burgess and Ligrani [3] at several different Reynolds numbers with $H/D = 1.0$, $d/D = 0.2$, and $D/S = D/Pi = 0.618$, in Fig. 5. The comparison is also made for average friction factor in Fig. 6. Although some deviations from the experimental data are shown especially for friction factor, the agreements are generally acceptable for the purpose of shape optimization. In the present optimization, Reynolds number based on channel height with 25 °C air is 22,500.

Table 1
Design variables and ranges

Design variable	Lower bound	Upper bound
H/D	0.2	1.0
d/D	0.1	0.3
D/S	0.4	0.7

Ranges of design variables are listed in Table 1. Twenty sampling points are selected by Latin Hypercube Sampling (LHS). Numerical optimizations have been performed in the range of 0.0 to 0.11 of the weighting factor.

Figs. 7 and 8 show results of sensitivity analyses for two components of the objective function. Here, the percent change

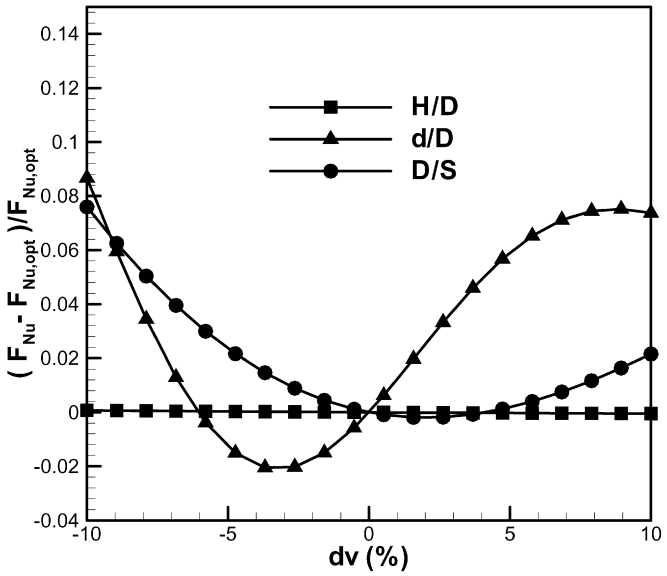

Fig. 7. Sensitivity analysis of F_{Nu} for optimal shape ($\beta = 0.09$).

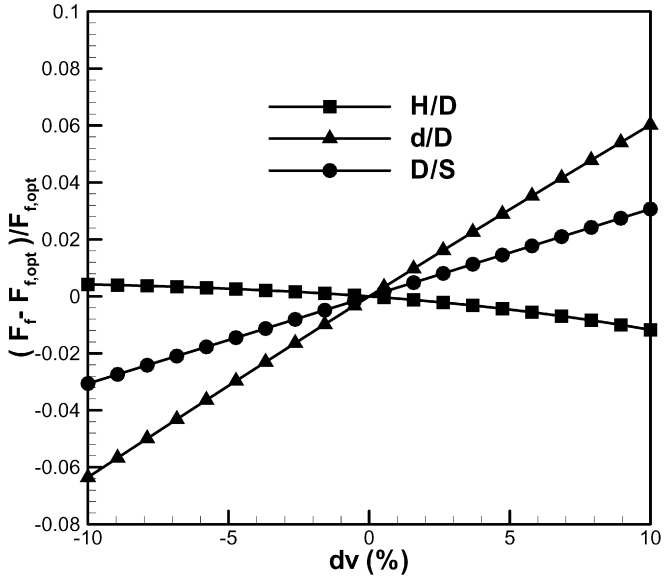

Fig. 8. Sensitivity analysis of F_f for optimal shape ($\beta = 0.09$).

of each design variable, dv is varied within $\pm 10\%$ of the optimal value, and the subscript, opt represents the value at optimal shape for $\beta = 0.09$. From these sensitive analyses, it is evident that the heat transfer and friction coefficients are most sensitive to d/D, and insensitive to H/D, which is confirmed by the experiment performed by Burgess and Ligrani [3]. The results of sensitivity analysis for the objective function with $\beta = 0.09$ are shown in Fig. 9. It is found that the objective function is most sensitive to the ratio of dimple depth to dimple print diameter as expected from Figs. 7 and 8.

Table 2 shows the results of optimization for $\beta = 0.09$. The reference shape was selected arbitrarily among the sampling points. The average Nusselt number is increased by 58% in comparison with the reference shape. But, the value of friction-loss related term (F_f) is also increased by 7%. It is noted that

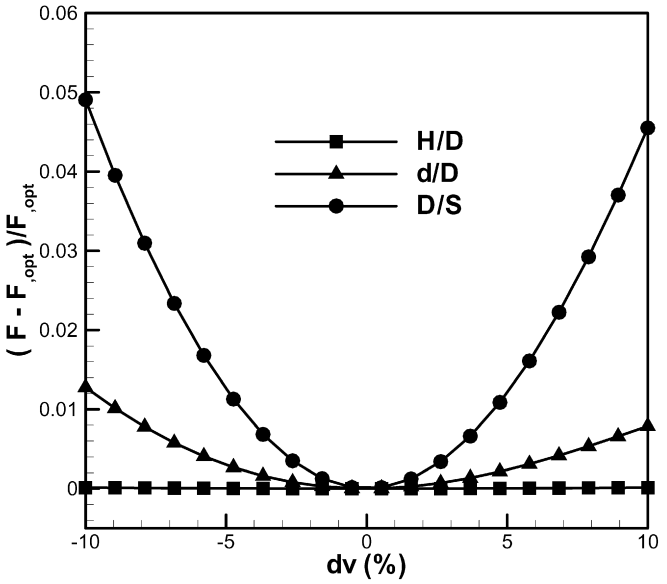

Fig. 9. Sensitivity analysis of objective function for optimal shape ($\beta = 0.09$).

Table 2
Results of optimization for $\beta = 0.09$

	Design variable			Nu_a	F_f	F
	H/D	d/D	D/S			
Reference	1.00	0.20	0.62	2.03	1.61	0.63
Optimum	0.39	0.30	0.59	3.21	1.72	0.47

the decrease in H/D is remarkable in comparison with the reference shape. This is consistent with the experimental results obtained by Mahmood and Ligrani [2], who reported that heat transfer rate increases as H/D ratio decreases. Finally, the objective function is reduced by 25% in comparison with the reference shape.

Distributions of local Nusselt number on dimpled walls are shown in Fig. 10. In both of the cases, heat transfer rate decreases abruptly just behind the front rim of the dimple due to flow separation, and increases downstream to reach the maximum near rear rim of the dimple. The distributions are not symmetric due to the asymmetric flow structure. Isaev and Leont'ev [23] reported that the turbulent flow past deep dimples ($d/D = 0.22-0.24$) becomes asymmetric under conditions of the absence of a performed symmetric vortex structure.

Fig. 11 shows the flow patterns of spreading over surfaces of the reference and the optimum dimples with asymmetric vortex structures. Compared to the structure shown in Fig. 11(a) for the reference shape, the streamlines over the optimized dimpled surface (Fig. 11(b)) show strongly asymmetric vortex structure. Fig. 12 shows the flow structures in the optimal and the reference dimples. Flow separation occurs at the front rim of the dimple, and, reattachment of the flow occurs on the rear part of the dimple in the case of optimum shape. But, in case of the reference shape (Fig. 12(a)), the flow pattern in dimple is complicated, since this plane is located near the border of vortex pair in dimple as shown in Fig. 11(a).

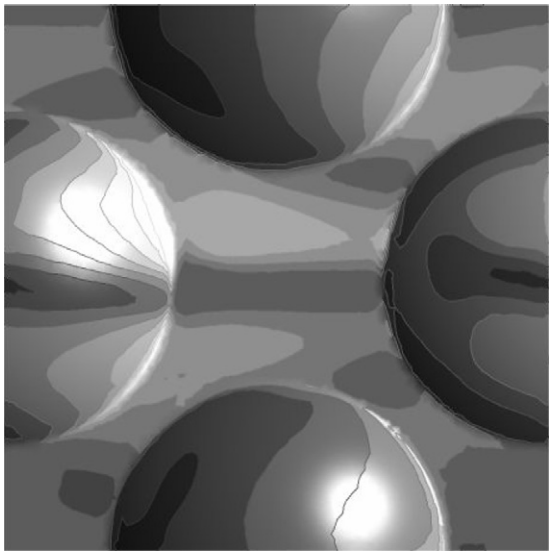

(a)

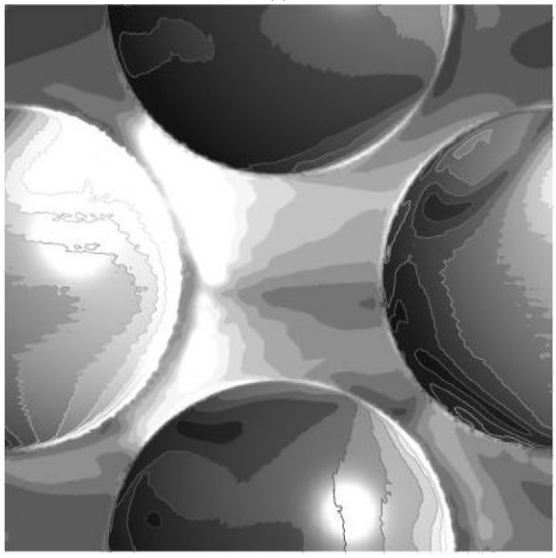

(b)

Fig. 10. Nusselt number distributions ($\beta = 0.09$): (a) reference, (b) optimum.

In most of the recirculation region, heat transfer rate is lower than that at the upstream of the dimple as shown in Fig. 10. It is found in Figs. 10, 11 and 12 that the heat transfer rate increases rapidly on the rear part of the dimple surface because of the flow reattachment and this continues till the rear rim of the dimple is reached in both cases. This is also confirmed by Fig. 13, where local Nusselt number distributions along the dimple diagonal in streamwise direction are compared for reference and optimum shapes. The dotted circles on the curves in Fig. 13 indicate the dimple boundaries, and $x = 0$ is located at the center of dimple as shown in Fig. 1. It is obvious that the heat transfer rate reaches a small peak at the front rim of the dimple in

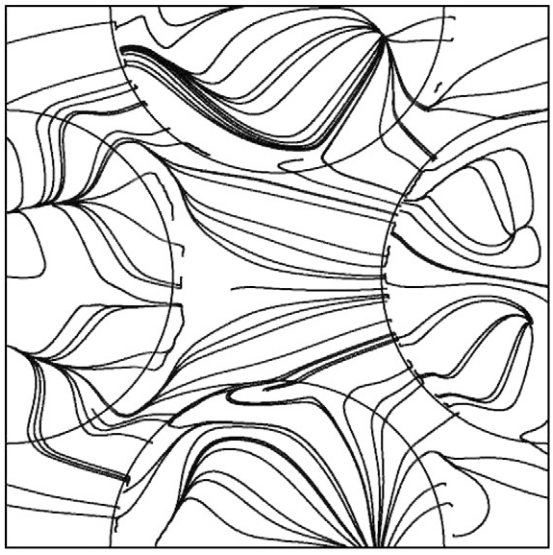

(a)

(b)

Fig. 11. Streamline distributions ($\beta = 0.09$): (a) reference, (b) optimum.

both cases. In case of the optimum shape, the heat transfer rate decreases sharply just downstream of the front rim to reach the minimum in very short distance, and increases again to the maximum at the rear rim of the dimple, which is followed by a rapid decrease. However, in case of the reference shape, the sharp decrease in heat transfer rate just behind the front rim is not found, but start of increase in heat transfer rate is quite delayed in the dimple compared to the case of the optimum shape. Thus, the Nusselt number distribution in the optimal channel maintains the higher level in the region between the dimples and in the downstream part of dimple in comparison with the reference channel.

Variations of the optimal design variables are plotted for different weighting factors in Fig. 14. The design variables in this figure are those normalized in the ranges shown in Table 1, and have the values between 0.0 and 1.0. With the increase of weighting factor, in other words, as designer's purpose is shifted to the reduction of pressure drop, d/D and D/S slightly

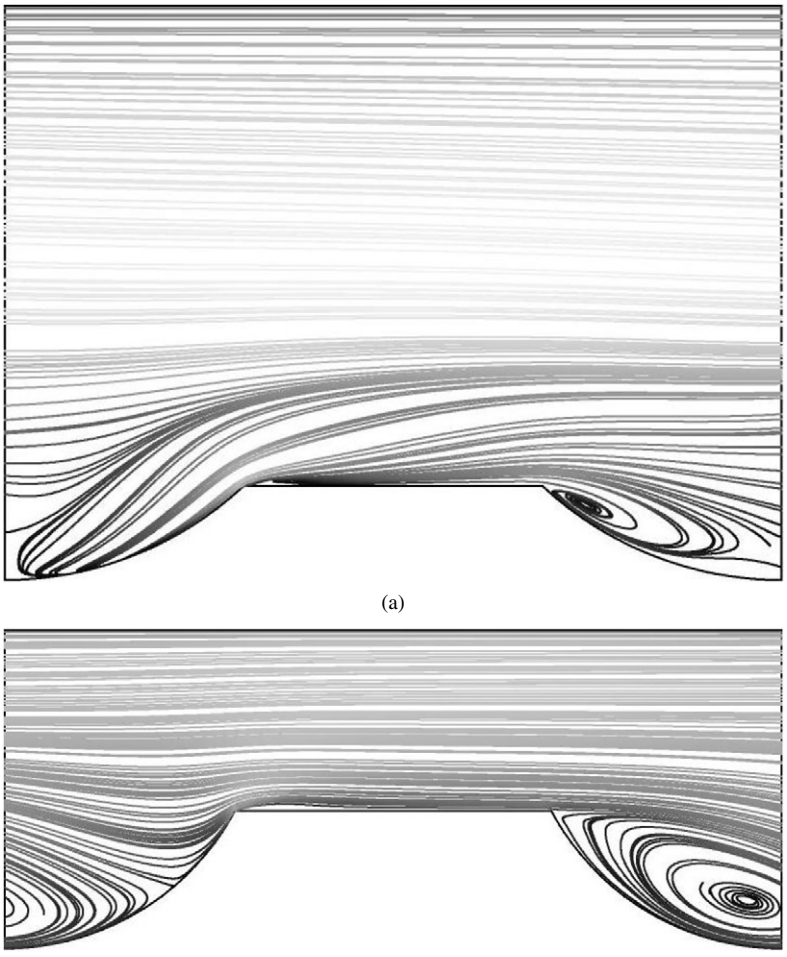

(a)

(b)

Fig. 12. Streamlines on cross section including streamwise dimple diagonal ($\beta = 0.09$): (a) reference, (b) optimum.

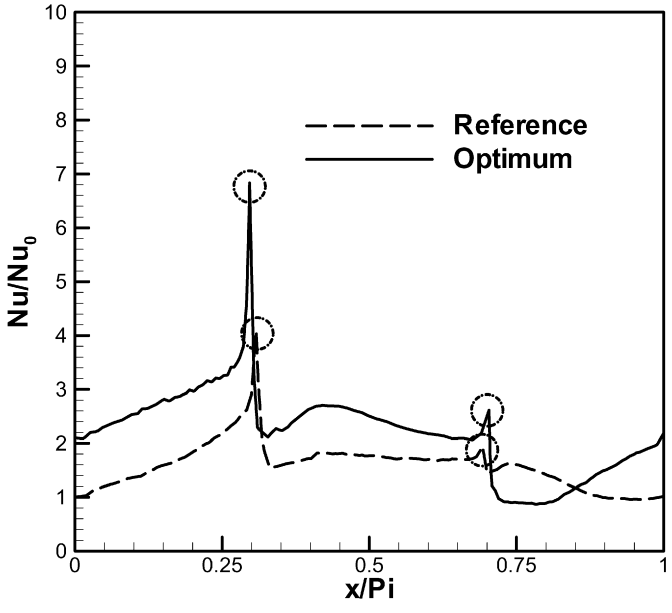

Fig. 13. Nusselt number distributions along the streamwise dimple diagonal for reference and optimum shapes ($\beta = 0.09$) (dotted circles indicate the dimple boundaries).

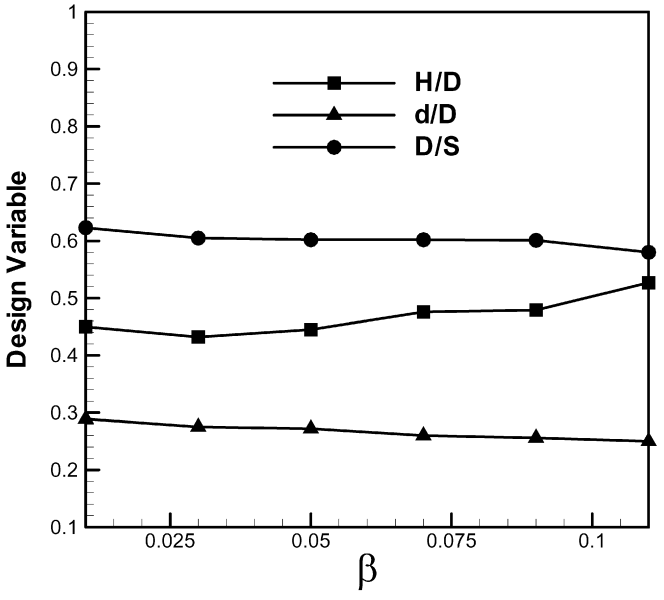

Fig. 14. Variations of optimal design variables with weighting factor.

decrease, but H/D increases. Since the friction loss, i.e., the pressure drop across the dimple decreases as the dimple depth is reduced, the optimal value of d/D moves toward the smaller

value with the increasing of weighting factor. The optimum value of H/D increases with the weighting factor, because friction loss decreases as the channel height is increased.

5. Conclusions

A staggered dimpled channel has been optimized by compromising enhancement of heat transfer and reduction of pressure loss by Kriging model based optimization method coupled with Reynolds-averaged Navier–Stokes analyses of fluid flow and heat transfer. Computational results for average Nusselt numbers as well as average friction factors show reasonable agreements with the experimental data. The objective function is defined as a combination of heat transfer and friction loss related terms with a weighting factor. Twenty sampling points with three design variables are selected by Latin Hypercube Sampling technique. It is found that both the heat transfer and friction loss related components of objective function are most sensitive to the ratio of dimple depth to dimple print diameter. The optimal values of design variables were obtained by varying the weighting factor. As the weighting factor increases, in other words, as the design emphasis is shifted towards the reduction in friction loss, optimal values of the ratio of dimple depth to dimple print diameter and the ratio of dimple print diameter to distance between dimples decrease, but the ratio of channel height to dimple print diameter increases.

Acknowledgements

This work was supported by grant No. R01-2006-000-10039-0 from the Basic Research Program of the Korea Science & Engineering Foundation.

References

[1] P.M. Ligrani, M.M. Oliveira, T. Blaskovich, Comparison of heat transfer augmentation techniques, AIAA J. 41 (2003) 337–362.
[2] G.I. Mahmood, P.M. Ligrani, Heat transfer in a dimpled channel: combined influences of aspect ratio, temperature ratio, Reynolds number, and flow structure, Int. J. Heat Mass Transfer 45 (2002) 2011–2020.
[3] N.K. Burgess, P.M. Ligrani, Effects of dimple depth on Nusselt numbers and friction factors for internal cooling channel, in: ASME Turbo Expo 2004, Vienna, Austria, 2004, ASME Paper GT2004-5432.
[4] J. Park, P.R. Desam, P.M. Ligrani, Numerical predictions of flow structure above a dimpled surface in a channel, Numerical Heat Transfer A 45 (2004) 1–20.
[5] J. Park, P.M. Ligrani, Numerical predictions of heat transfer and fluid flow characteristics for seven different dimpled surfaces in a channel, Numerical Heat Transfer A 47 (2005) 209–232.
[6] K.Y. Kim, J.Y. Choi, Shape Optimization of a dimpled channel to enhance turbulent heat transfer, Numerical Heat Transfer A 48 (2005) 901–915.
[7] H.M. Kim, K.Y. Kim, Shape optimization of three-dimensional channel roughened by angled ribs with RANS analysis of turbulent heat transfer, Int. J. Heat Mass Transfer 49 (2006) 4013–4022.
[8] K.Y. Kim, Y.M. Lee, Design optimization of internal cooling passage with V-shaped ribs, Numerical Heat Transfer A (2007), in press.
[9] J. Sacks, W.J. Welch, T.J. Mitchell, H.P. Wynn, Design and analysis of computer experiments, Statistical Science 4 (1989) 409–435.
[10] A.J. Booker, Cases studies in design and analysis of computer experiments, in: Proceedings of the Section on Physics and Engineering Sciences, 1996.
[11] A.A. Guinta, Aircraft multidisciplinary design optimization using design of experiments theory and response surface model, PhD thesis and MAD center report no 97-05-01, Department of Aerospace and Ocean Engineering, Virginia, Polytechnic Institute and State University, Blacksburg, VA, 1997.
[12] K. Park, P.K. Oh, H.J. Lim, The application of CFD and Kriging method to an optimization of heat sink, Int. J. Heat Mass Transfer 49 (2006) 3439–3447.
[13] CFX-11.0 Solver Theory, Ansys Inc., 2006.
[14] B.W. Webb, S. Ramadhyani, Conjugate heat transfer in a channel with staggered ribs, Int. J. Heat Mass Transfer 28 (1985) 1679–1687.
[15] F.R. Menter, Two-equation eddy-viscosity turbulence models for engineering applications, AIAA J. 32 (1994) 1598–1605.
[16] J.E. Bardina, P.G. Huang, T. Coakley, Turbulence modeling validation, AIAA Paper 97-2121, 1997.
[17] Y.G. Lai, R.M.C. So, Near-wall modeling of turbulent heat fluxes, Int. J. Heat Mass Transfer 33 (1990) 1429–1440.
[18] D.L. Gee, R.L. Webb, Forced convection heat transfer in helically rib-roughened tubes, Int. J. Heat Mass Transfer 23 (1980) 1127–1136.
[19] J.C. Han, J.S. Park, C.K. Lei, Heat transfer enhancement in channels with turbulence promoters, J. of Eng. Turbines Power 107 (1985) 628–635.
[20] B.S. Petukhov, in: Advances in Heat Transfer, vol. 6, Academic Press, New York, 1970, pp. 503–504.
[21] M.D. McKay, R.J. Beckman, W.J. Conover, A comparison of three methods for selecting values of input variables in the analysis of output from a computer code, Technometrics 21 (1979) 239–245.
[22] MATLAB®, The language of technical computing, Release 14, The MathWorks Inc., 2005.
[23] S.A. Isaev, A.I. Leont'ev, Numerical simulation of vortex enhancement of heat transfer under conditions of turbulent flow past a spherical dimple on the wall of a narrow channel, High Temperature 41 (2003) 665–679.